Large-format SPAD image sensors for biomedical and HEP applications

Edoardo Charbon & Claudio Bruschini
AQUA Lab
Advanced Quantum Architecture Laboratory, School of Engineering, EPFL
1015 Lausanne, Switzerland

E-mail: edoardo.charbon@epfl.ch

Keywords: single-photon avalanche diode, SPAD, LiDAR, 3D stacking, time-of-flight sensing, 3D integration.

Abstract– CMOS SPAD image sensors have reached 1Mpixel in 2020 after two decades of evolution. The core peculiarity of SPADs is an excellent timing resolution, at the center of the success of these sensors in time-resolved imaging. Applications have literally exploded, with 3D-stacking enabling deep-learning processors and complex processing *in situ*, hence reducing power consumption. Another recent trend is the use of SPADs in quantum imaging and quanta burst photography, that are notoriously computationally intensive. Recent examples include particle sensing in HEP experiments, FLIM/FRET, and various super-resolution microscopy styles. In this paper we review all these trends and the newest results achieved with advanced technologies.

Introduction

Single-photon avalanche diodes (SPADs) are photodiodes biased above breakdown, where sustained avalanche can be achieved through impact ionization upon electron-hole generation caused by photons or by thermal generation [1,2]. Fig. 1 shows the operation of a photodiode in conventional mode and in Geiger mode. The figure also shows the typical cross-section of the SPAD, comprising an anode, cathode, and guard rings to prevent early edge breakdown.

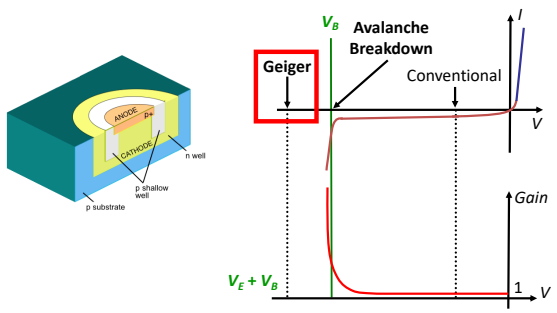

Fig. 1. Single-photon avalanche diode principle and cross-section of a SPAD.

In this mode of operation, SPADs can detect single photons or perform photon counting by generating a digital signal upon photon detection. This operation occurs in a few nanoseconds, yielding photon detection

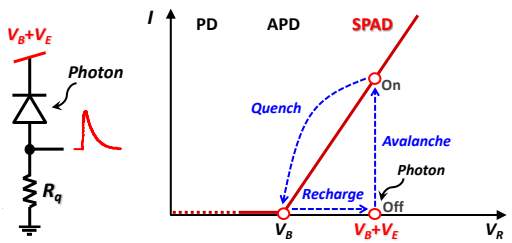

Fig. 2. SPAD detection cycle.

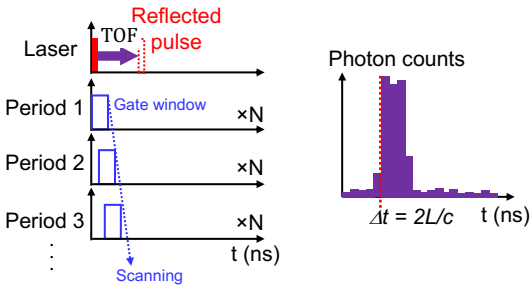

Fig. 3. Time gating technique for lifetime reconstruction. The time-of-flight (TOF) of the photon reflection may also be extracted. The time gate may be significantly longer than the histogram bin, which is only determined by the delay of the gating process.

at high timing resolution [3-8]; it is illustrated in Fig. 2, where passive quenching is performed with a ballast resistor to avoid destruction of the SPAD and to transform the avalanche current into a voltage, which, in turn, can be converted into a digital signal [9,10].

SPADs can also be gated, i.e. activated in a few tens of picoseconds and deactivated as fast. Time gating is used to reconstruct fast processes, such as fluorescence response, to extract lifetime, for instance [11-17]. Fluorescence lifetime imaging microscopy (FLIM) is one such modality, for which SPADs can be effectively used. Fig. 3 shows the process of reconstruction achieved by successive exposures of a molecule to light pulses and subsequent histogram building for lifetime. As shown in the figure, the histogram bin size is determined by the minimum delay achieved by the gating process, even if the time gate itself could be longer, typically several nanoseconds.

Large-format SPAD image sensors

In order to achieve widefield FLIM, one can either scan the scene in a confocal microscope or use a large number of pixels synchronized with a laser source. In the latter case a high frame rate may be achieved, provided that the gate skew is small over the whole SPAD array. To

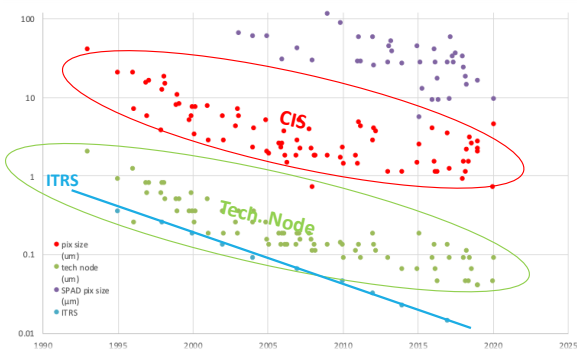

Fig. 4. SPAD pitch evolution (in purple) vs. CIS technology. Source: A. Theuwissen, H.A.R. Homulle, and E. Charbon.

achieve large pixel counts, one needs to reduce SPAD size and pixel pitch [15]. Fig. 4 shows pitch evolution in SPADs, compared to conventional image sensor technology over the years following the ITRS feature size reduction. As can be seen from the figure, SPADs have followed CMOS IS (CIS) pitch reduction with some delay, mostly due to the constraints imposed on the device by high voltages and the need for lower doping profiles that prevented the use of more advanced CMOS technology nodes [18-25]. In addition, new pixel

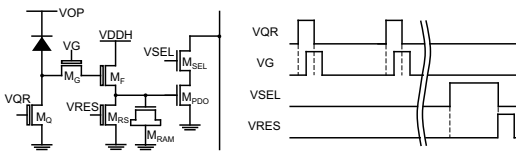

Fig. 5. MegaX pixel A (7T).

architectures were required to perform biomedical imaging [26-29] or quantum key distribution [30].

As an example, Fig. 5, shows the design of a gated SPAD in 180nm CIS technology achieving a pitch of 9.4µm in the chip MegaX. The pixel is an evolution of [31] and it comprises a quenching mechanism through transistor M_Q and gating through M_G, M_F, and M_{RS}, which resets the pixel [32]. The information of the detection of a photon is stored in M_{RAM} and read out through M_{PDO} and M_{SEL}. The MegaX chip is shown in Fig. 6, which includes the first SPAD array of 1Mpixel ever achieved.

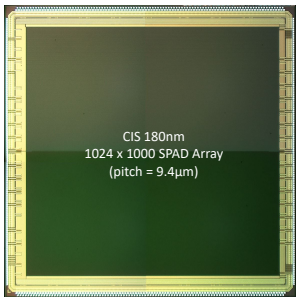

Fig. 6. The MegaX chip [32].

Fig. 7 shows the characterization of the MegaX chip in terms of dark count rate (DCR) and photon detection probability (PDP) as a function of population, excess bias, and temperature. A second pixel (Pixel B) was also implemented in this architecture that enabled a better fill factor thanks to the sharing of readout transistors groups of 2×2 pixels.

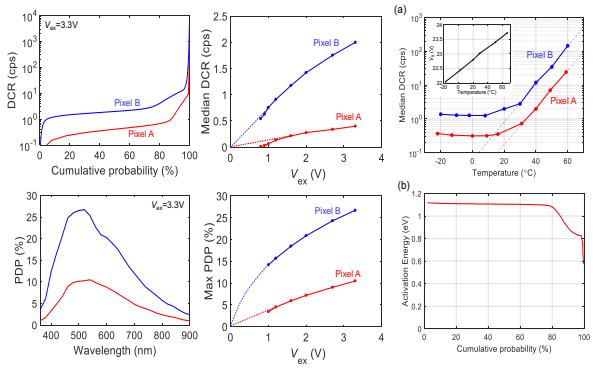

Fig. 7. MegaX characterization.

3D-stacked architectures

In order to enable further pixel pitch reduction, one can stack two or more chips, one hosting the detectors and one the electronics supporting them.

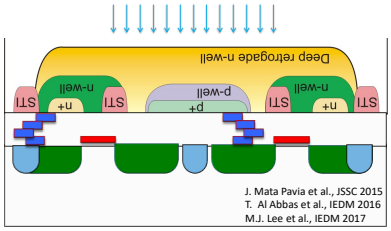

Fig. 8. Backside-illuminated (BSI) SPAD and 3D-stacked configuration.

A simplified cross-section of such a scheme can be seen in Fig. 8, which shows a SPAD cross-section, flipped, thinned and hybrid-bonded with a chip implemented in the same or in another technology node. This structure is known as backside-illuminated (BSI) 3D-stacked configuration [20,33,34]. The bottom-tier chip may host quenching and gating transistors but it may also include much more electronics, including advanced processing and even machine-learning engines. 3D-stacked chips may also be built to implement frontside-illuminated (FSI) SPADs [35]. In this case, the SPAD will require a through-silicon via (TSV), to establish the connection with the bottom-tier chip. Though the principle is the same, FSI SPADs have different performance, especially in the PDP and wavelength response than BSI SPADs. Fig. 9 shows a comparison between FSI and BSI SPADs as a function of wavelength and excess bias.

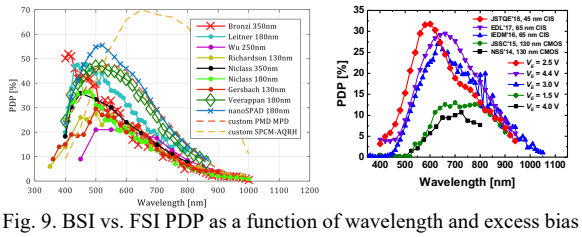

Fig. 9. BSI vs. FSI PDP as a function of wavelength and excess bias [20].

Further pitch reduction can be achieved with techniques ranging from guard ring sharing to the use of more advanced CMOS technology nodes, whereas the currently smallest pitch was demonstrated in [36]. Fig. 10 shows a demonstration of small pitch using guard ring sharing (left) and with the use of a BCD 55-nm technology node (right) [37-39].

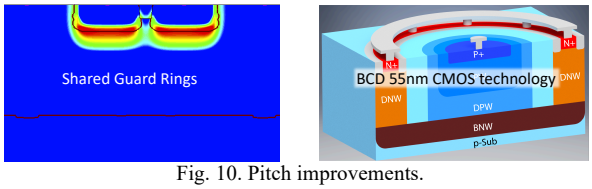

Fig. 10. Pitch improvements.

Biomedical and HEP applications

In FLIM, large-format SPAD image sensors have been successfully employed in recent years [26]. Phasors have also been successfully used to represent lifetime with data obtained by sensors like SwissSPAD2 [31]. Phasors are derived from the lifetime as a projection to the sine and cosine planes as seen in Fig. 11a. Fig. 11b

Tab. 1. Summary of FSI SPAD performance found in [38].

Comparative Table									
	Technology (nm)	Diameter μm	V_{EX}/V_{BD} (V)	Peak PDP (%) @λ (nm)	PDP (%) @850 nm	DCR/unit area ($cps/\mu m^2$)	AP (%)	Jitter (ps)	FoM$_T$ [44]
Ghioni [7]	Custom Thin	50-200	5-10/30-35	52-68 @550	12-15	0.4-1.6^a	2^b	35^c	1.88E+11
Gulinatti [8]	Custom RE	50	20/45-55	58 @650	28	0.3^d	N/A	93^c	N/A
Villa [16]	350	10-500	2-6/25	37-53 @450	2-4.5	0.05^a	1^e	90^f	6.52E+11
Leitner [17]	180	10	1-3.3/21	35-47 @450	N/A^g	0.3-1.8^a	N/A	N/A	N/A
Veerappan [18]	180	12	2-10/23.5	24-48 @480	3-8	0.16-176^a	0.03-0.3^h	112-88^i	1.37E+9
Verappan [19]	180	12	1-4/14	23-47 @480	4-7	0.28-16^d	0.2^j	161-141^i	2.78E+9
Veerappan [21]	180	12	1-12/25	18-47 @520	2-8	0.2-6^d	7.2^k	139-101^i	5.88E+9
Xu [22]	150	10	2-5/19	24-32 @450	2-3.5	0.1-1	1-13^l	42^m	1.33E+11
Lee [20]	140(SOI)	12	0.5-3/11	12-25 @500	2.5-7	0.9-260	1.7^n	65°	1.17E+9
Richardson [13]	130	8	0.6-1.4/14	18-28 @500	3-5	0.24-0.6^a	0.02^p	200^q	9.04E+9
Richardson [12]	130	8	0.2-1.2/12-18	18-33 @450	2-5	0.4-0.8	0.02^r	237-184^s	4.01E+10
Niclass [10]	130	10	1-3.5/10	31-41 @450	3	120-1300^d	N/A	144^i	N/A
Niclass [43]	180	25	5/20.5	64.8 @610^{ii}	24	0.6	0.49^{dd}	190	1.83E+11
Gersbach [11]	130	4.3	1-2/9	18-30 @480	3.5-5	1.5-11.5	<1^t	125^i	3.89E+9
Charbon [15]	65	8	0.05-0.4/9	2-5.5 @420	0.2-0.4	340-15.6k^a	<1^u	235^i	3.71E+5
Sanzaro(A) [24]	160(BCD)	10-80	3-9/36	31-58 @450	2.5-6.5	0.12-0.2^v	0.43-1.59^w	39-28^c	9.12E+11
Sanzaro(B) [24]	160(BCD)	10-80	3-9/25	2-47 @450	2.5-6.5	0.1-0.18^v	0.02-0.14^w	36-28^c	7.9E+11
Sanzaro(C) [24]	160(BCD)	10-80	3-9/26	55-71 @490	6-9	0.13-0.19^v	0.41-1.26^w	41-28^c	1.15E+12
Pellegrini [25]	40	18.36	1/15.5	45 @460$^+$	5	N/A†	0.1	170*	N/A
Nolet [5]	65	20	1.75/9.9	8 @470	N/A	2.8k	<10	7.8$^\sharp$	N/A
Webster [14]	90	6.4	14.9/2.4	44 @700	22	8.1k	0.375	84	N/A
[38]	**180**	**25-100**	**1-11/22**	**25-55@480**^{2}	**3-8.4**^{x}	**0.06-0.23**^{y}	**~0.12-3**^{z}	**12.1**^{1}	**2.78E+13**

^{a}At 20°C.^{b}200μm-diameter, at 25°C, 80 ns dead time,V$_{EX}$=5V.^{c}820 nm wavelength.^{d}At 25°C.^{dd}24 ns dead time. ^{e}30 μm-diameter, at 25°C, 40 ns dead time,V$_{EX}$=5 V, integrated AQC. ^{f}A time resolution of 28-37 ps FWHM and a diffusion tail of 160-340 ps were demonstrated in Ref. [45] using the substrate bias as a trade-off parameter between jitter and diffusion tail.^{g}PDE=10-13% at 800 nm.^{h}300 ns dead time, V$_{EX}$=2-10 V.^{i}637 nm wavelength.^{ii}Substrate not isolated SPAD. ^{j}300 ns dead time, V$_{EX}$=4V.^{k}300 ns dead time, V$_{EX}$=11 V.^{l}50 ns dead time, V$_{EX}$=1.5-5 V.^{m}831 nm wavelength.^{n}200 ns dead time, V$_{EX}$=2V.^{o}405 nm wavelength.^{p}200 ns dead time,V$_{EX}$=2V.^{q}815 nm wavelength.^{r}50 ns dead time.^{s}470 nmwavelength.^{t}180 ns dead time.^{u}5μs dead time.^{v}At 300 K.^{w}30μm-diameter, at 300 K, 50 ns dead time.^{x}Measured between 1V and 6V excess bias at 25°C.^{y}25μm-diameter at 20°C measured at 1 V and 6 V excess bias.^{z}For a dead time of 3 ns on the 25 μm-diameter and 100 μm-diameter SPADs at 25°C and 6 V excess bias.* 1 V excess bias, room temperature and 850nm laser.$^+$Using microlenses.†About 100 cps at room temperature at 1V excess bias.$^\sharp$410 nm laser.^{1}25μm-diameter at 20°C with an excess bias of 6V.^{2} value taken at 1 V and 6 V excess bias.

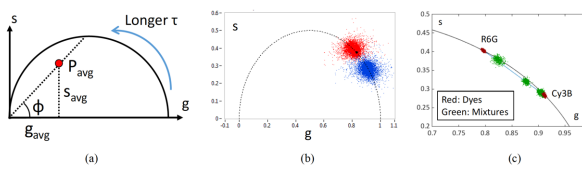

Fig. 11. Phasor interpretation in SPAD image sensors. (a) Principle. (b) Phasor plots for Rhodamine 6G: R6G (τ =4.08ns) and Cy3B (τ =2.8ns) solutions. (c) Dye mixture analysis of Cy3B and R6G with 5 different volume fractions.

shows an example of two fluorophores, while Fig. 11c shows the result of mixture of dyes. All these measurements were obtained with 16 gate positions and 13.1ns gate width.

Recently, more powerful SPAD sensors have appeared, with shorter gate width, as low as 1ns, and faster continuous readout speed [40]. PDP has been enhanced in red and NIR, while dynamic range and signal-to-noise ratio have been modeled and used in advanced applications [41-44].

In high energy physics, SPAD image sensors can be used to track high-energy particles directly without use of scintillators, thus achieving the best possible timing resolution in the extraction of the time-of-flight of the particles and their trajectory. In [37] for instance pions have been detected directly using fast SPADs; in the presence of an array of fast SPADs the trajectory could have been derived more extensively and thus more research is needed in this field.

Conclusions

Large-format SPAD image sensors are now a reality, with SPAD multi-megapixels being marketed by Panasonic and Canon. While individual SPADs have reached a timing resolution as high as 7.5ps (FWHM) and a maximum PDP of over 60% with a dead time as low as 1.5ns, large arrays can be used already in a number of applications, including FLIM and phasors. Tab. 1 summarizes the current state-of-the-art in SPAD's salient performance measures. We expect that the introduction of 3D-stacked SPAD image sensors will enable important advances in computationally intensive image sensing, adding more powerful computational capabilities at chip, pixel cluster, or even pixel level.

References

[1] S. Cova, M. Ghioni, A. Lacaita, C. Samori, and F. Zappa, "Avalanche photodiodes and quenching circuits for single-photon detection," Applied Optics, vol. 35, no. 12, pp. 1956–1976, 1996.

[2] F. Ceccarelli, G. Acconcia, A. Gulinatti, M. Ghioni, I. Rech, and R. Osellame, "Recent advances and future perspectives of single photon avalanche diodes for quantum photonics applications," Advanced Quantum Technologies, p. 2000102, 2020.

[3] S. Cova, A. Lacaita, M. Ghioni, G. Ripamonti, and T. Louis, "20-ps timing resolution with single-photon avalanche diodes," Review of Scientific Instruments, vol. 60, no. 6, pp. 1104–1110, 1989.

[4] A. Spinelli, M. A. Ghioni, S. D. Cova, and L. M. Davis, "Avalanche detector with ultraclean response for time-resolved photon counting," IEEE Journal of Quantum Electronics, vol. 34, no. 5, pp. 817–821, 1998.

[5] F. Nolet, S. Parent, N. Roy, M.-O. Mercier, S. Charlebois, R. Fontaine, and J.-F. Pratte, "Quenching circuit and SPAD integrated in CMOS 65nm with 7.8 ps FWHM single photon timing resolution," Instruments, vol. 2, p. 19, Sep. 2018.

[6] M. Ghioni, S. Cova, A. Lacaita, and G. Ripamonti, "New silicon epitaxial avalanche diode for single-photon timing at room temperature," Electronics Letters, vol. 24, no. 24, pp. 1476–1477, 1988.

[7] M. Ghioni, A. Gulinatti, I. Rech, F. Zappa, and S. Cova, "Progress in silicon single-photon avalanche diodes," IEEE Journal of Selected Topics in Quantum Electronics, vol. 13, no. 4, pp. 852–862, 2007.

[8] A. Gulinatti, I. Rech, F. Panzeri, C. Cammi, P. Maccagnani, M. Ghioni, and S. Cova, "New silicon SPAD technology for enhanced red sensitivity, high-resolution timing and system integration," Journal of Modern Optics, vol. 59, no. 17, pp. 1489–1499, 2012.

[9] A. Rochas, M. Gani, B. Furrer, P. Besse, R. Popovic, G. Ribordy, and N. Gisin, "Single photon detector fabricated in a complementary metal–oxide–semiconductor high-voltage technology," Review of Scientific Instruments, vol. 74, no. 7, pp. 3263–3270, 2003.

[10] C. Niclass, M. Gersbach, R. Henderson, L. Grant, and E. Charbon,

"A single photon avalanche diode implemented in 130-nm CMOS technology," IEEE Journal of Selected Topics in Quantum Electronics, vol. 13, no. 4, pp. 863–869, 2007.

[11] M. Gersbach, C. Niclass, E. Charbon, J. Richardson, R. Henderson, and L. Grant, "A single photon detector implemented in a 130nm CMOS imaging process," in European Solid-State Device Research Conference, pp. 270–273, 2008.

[12] J. A. Richardson, E. A. G. Webster, L. A. Grant, and R. K. Henderson, "Scaleable single-photon avalanche diode structures in nanometer CMOS technology," IEEE Trans. Electron Devices, vol. 58, no. 7, pp. 2028–2035, Jul. 2011.

[13] J. A. Richardson, L. A. Grant, and R. K. Henderson, "Low dark count single-photon avalanche diode structure compatible with standard nanometer scale CMOS technology," IEEE Photonics Technology Letters, vol. 21, no. 14, pp. 1020–1022, 2009.

[14] E. A. G. Webster, J. A. Richardson, L. A. Grant, D. Renshaw, and R. K. Henderson, "A single-photon avalanche diode in 90-nm CMOS imaging technology with 44% photon detection efficiency at 690 nm," IEEE Electron Device Letters, vol. 33, no. 5, pp. 694–696, 2012.

[15] E. Charbon, H. Yoon, and Y. Maruyama, "A Geiger mode APD fabricated in standard 65nm CMOS technology," in 2013 IEEE International Electron Devices Meeting, pp. 27.5.1–27.5.4, 2013.

[16] F. Villa, D. Bronzi, Y. Zou, C. Scarcella, G. Boso, S. Tisa, A. Tosi, F. Zappa, D. Durini, S. Weyers, U. Paschen, and W. Brockherde, "CMOS SPADs with up to 500μm diameter and 55% detection efficiency at 420nm," Journal of Modern Optics, vol. 61, no. 2, pp. 102–115, 2014.

[17] T. Leitner, A. Feiningstein, R. Turchetta, R. Coath, S. Chick, G. Visokolov, V. Savuskan, M. Javitt, L. Gal, I. Brouk, S. Bar-Lev, and Y. Nemirovsky, "Measurements and simulations of low dark count rate single photon avalanche diode device in a low voltage 180-nm CMOS image sensor technology," IEEE Transactions on Electron Devices, vol. 60, no. 6, pp. 1982–1988, 2013.

[18] C. Veerappan and E. Charbon, "A substrate isolated CMOS SPAD enabling wide spectral response and low electrical crosstalk," IEEE Journal of Selected Topics in Quantum Electronics, vol. 20, no. 6, pp. 299–305, 2014.

[19] C. Veerappan and E. Charbon, "CMOS SPAD based on photo-carrier diffusion achieving PDP >40% from 440 to 580 nm at 4 V excess bias," IEEE Photonics Technology Letters, vol. 27, pp. 2445–2448, 2015.

[20] M.-J. Lee, A.R. Ximenes, P. Padmanabhan, T.-J. Wang, K.-C. Huang, Y. Yamashita, D.N. Yaung, E. Charbon, "High-Performance Back-Illuminated Three-Dimensional Stacked Single-Photon Avalanche Diode Implemented in 45-nm CMOS Technology," IEEE Journal of Selected Topics in Quantum Electronics, vol. 24, no. 6, pp. 3801809, 2018.

[21] C. Veerappan and E. Charbon, "A low dark count p-i-n diode based SPAD in CMOS technology," IEEE Transactions on Electron Devices, vol. 63, pp. 65–71, 2016.

[22] H. Xu, L. Pancheri, G.-F. D. Betta, and D. Stoppa, "Design and characterization of a p+/n-well SPAD array in 150nm CMOS process," Optics Express, vol. 25, no. 11, pp. 12 765–12 778, May 2017.

[23] C. Veerappan, "Single-photon avalanche diodes for cancer diagnosis," Ph.D. dissertation, Delft University of Technology, Delft, Netherlands, March. 2016.

[24] M. Sanzaro, P. Gattari, F. Villa, A. Tosi, G. Croce, F. Zappa, "Single-photon avalanche diodes in a 0.16 μm BCD technology with sharp timing response and red-enhanced sensitivity," IEEE Journal of Selected Topics in Quantum Electronics, vol. 24, no. 2, p. 3801209, 2017.

[25] S. Pellegrini, B. Rae, A. Pingault, D. Golanski, S. Jouan, C. Lapeyre, and B. Mamdy, "Industrialised SPAD in 40 nm technology," in IEEE International Electron Devices Meeting, pp. 16.5.1–16.5.4, 2017.

[26] C. Bruschini, H. Homulle, I. M. Antolovic, S. Burri, and E. Charbon, "Single-photon avalanche diode imagers in biophotonics: review and outlook," Light: Science & Applications, vol. 8, no. 1, p. 87, 2019.

[27] X. Michalet, A. Ingargiola, R. A. Colyer, G. Scalia, S. Weiss, P. Maccagnani, A. Gulinatti, I. Rech, and M. Ghioni, "Silicon photon counting avalanche diodes for single-molecule fluorescence spectroscopy," IEEE Journal of Selected Topics in Quantum Electronics, vol. 20, no. 6, pp. 248–267, 2014.

[28] G. Buller and A. Wallace, "Ranging and three-dimensional imaging using time-correlated single-photon counting and point-by-point acquisition," IEEE Journal of Selected Topics in Quantum Electronics, vol. 13, no. 4, pp. 1006–1015, 2007.

[29] M. A. Karami and M. Ansarian, "Neural imaging using single-photon avalanche diodes," Basic and Clinical Neuroscience Journal, vol. 8, no. 1, 2017.

[30] H. Takesue, E. Diamanti, C. Langrock, M. Fejer, and Y. Yamamoto, "10-GHz clock differential phase shift quantum key distribution experiment," Optics Express, vol. 14, no. 20, pp. 9522–9530, 2006.

[31] A. C. Ulku, C. Bruschini, I. M. Antolovi´c, Y. Kuo, R. Ankri, S. Weiss, X. Michalet, and E. Charbon, "A 512 × 512 SPAD image sensor with integrated gating for widefield flim," IEEE Journal of Selected Topics in Quantum Electronics, vol. 25, no. 1, pp. 1–12, 2019.

[32] K. Morimoto, A. Ardelean, M.-L. Wu, A. C. Ulku, I. M. Antolovic, C. Bruschini, and E. Charbon, "Megapixel time-gated SPAD image sensor for 2D and 3D imaging applications," Optica, vol. 7, no. 4, pp. 346–354, Apr. 2020.

[33] S. Lindner, S. Pellegrini, Y. Henrion, B. Rae, M. Wolf, and E. Charbon, "A high-PDE, backside-illuminated SPAD in 65/40-nm 3D IC CMOS pixel with cascoded passive quenching and active recharge," IEEE Electron Device Letters, vol. 38, no. 11, pp. 1547–1550, 2017.

[34] T. Al Abbas, N. A.W. Dutton, O. Almer, S. Pellegrini, Y. Henrion, R.K. Henderson, "Backside illuminated SPAD image sensor with 7.83μm pitch in 3D-stacked CMOS technology," IEEE International Electron Devices Meeting, 8.1.1-8.1.4, 2016.

[35] F. Gramuglia, A. Muntean, E. Venialgo, M.-J. Lee, S. Lindner, M. Motoyoshi; A. Ardelean; C. Bruschini, E. Charbon, "CMOS 3D-Stacked FSI Multi-Channel Digital SiPM for Time-of-Flight PET Applications," IEEE Nuclear Science Symposium, 2020.

[36] K. Morimoto and E. Charbon, "High fill-factor miniaturized SPAD arrays with a guard-ring-sharing technique," Optics Express, vol. 28, no. 9, pp. 13068-13080, 2020.

[37] F. Gramuglia, E. Ripiccini, C.A. Fenoglio, M.L. Wu, L. Paolozzi, C. Bruschini, E. Charbon, "Sub-10 ps Minimum Ionizing Particle Detection with Geiger-Mode APDs," arXiv:2111.09998v1, 2021.

[38] F. Gramuglia, M.-L. Wu, C. Bruschini, M.J. Lee, E. Charbon, "A Low-noise CMOS SPAD Pixel with 12.1 ps SPTR and 3 ns Dead Time," IEEE Journal of Selected Topics in Quantum Electronics, vol. 28, no. 2, pp. 1-9, 2021.

[39] F. Gramuglia, P. Keshavarzian, E. Kizilkan, C. Bruschini, S. Seng Tan, M. Tng, E. Quek, M.-J. Lee, E. Charbon, "Engineering Breakdown Probability Profile for PDP and DCR Optimization in a SPAD Fabricated in a Standard 55 nm BCD Process," IEEE Journal of Selected Topics in Quantum Electronics, vol. 28, no. 2, pp. 3802410, 2022.

[40] A.C. Ulku, A. Ardelean, P. Mos, C. Bruschini, E. Charbon, "A 500×500 Dual-Gate SPAD Imager with 100% Temporal Aperture and 1 ns Minimum Gate Width for FLIM and Phasor Imaging Applications," International Image Sensor Workshop, 2021.

[41] R. Ankri, A. Basu, A.C. Ulku, C. Bruschini, E. Charbon, S. Weiss, X. Michalet, "Single-Photon, Time-Gated, Phasor-Based Fluorescence Lifetime Imaging through Highly Scattering Medium," ACS Photonics, vol. 7, no. 1, pp. 68-79, 2019.

[42] D. Bronzi, F. Villa, S. Tisa, A. Tosi, and F. Zappa, "SPAD figures of merit for photon-counting, photon-timing and imaging applications: A review," IEEE Sensors Journal, vol. 16, no. 1, pp. 3–12, 2016.

[43] C. Niclass, H. Matsubara, M. Soga, M. Ohta, M. Ogawa, and T. Yamashita, "A NIR-sensitivity-enhanced single-photon avalanche diode in 0.18μm CMOS," in Proceedings of the International Image Sensor Workshop, Vaals, The Netherlands, 2015, pp. 8–11.

[44] I. M. Antolovic, C. Bruschini, and E. Charbon, "Dynamic range extension for photon counting arrays," Optics Express, vol. 26, no. 17, pp. 22 234–22 248, Aug 2018.